CHEMISTRY OF MATERIALS

pubs.acs.org/cm Article

Is Formamidinium Always More Stable than Methylammonium?

Haotong Wei,[†] Shangshang Chen,[†] Jingjing Zhao, Zhenhua Yu, and Jinsong Huang*

Cite This: https://dx.doi.org/10.1021/acs.chemmater.9b05101 Read Online

ACCESS | Metrics & More | Article Recommendations

ABSTRACT: Halide perovskite solar cells have achieved unprecedented progress in efficiency and high-throughput module manufacturing; however, the stability of perovskite devices remains to be a major obstacle for their commercialization. Among various instability sources in perovskite solar cells, methylammonium (MA) has been identified to limit the thermal stability of perovskites with different band gaps. Formamidinium (FA) ions are frequently used to partially or fully replace MA ions for improved stability. Here, we show that FA ions can be less stable in precursor solution than MA ions. The −CH═NH double bonds of FA ions gradually converted into −CH═O under light in solution despite the fact that this reaction is not obvious in the solid state. The generation of −CH═O is confirmed by the FTIR measurements. FA ions containing perovskite solution stored in the dark shows comparable device efficiency with a fresh perovskite solution, while light soaking of FA-containing perovskite solution greatly impairs the device efficiency, confirming the light-induced FA degradation. This study highlights the importance of precursor solution stability and arouses the attention to avoid illumination during device fabrication.

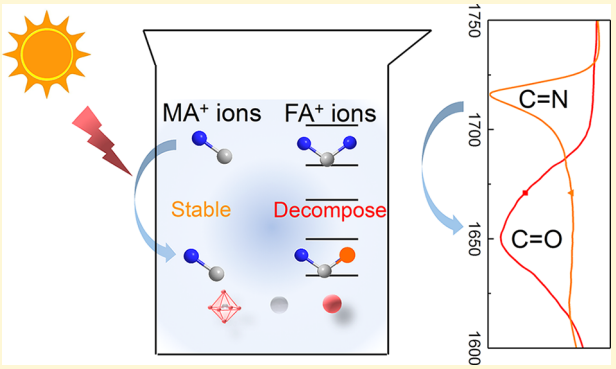

INTRODUCTION

Metal halide perovskites have attracted lots of attention as a new generation of optoelectronic materials, and the power conversion efficiency (PCE) of perovskite solar cells has been boosted rapidly within several years, benefiting from their unique physical and chemical properties.[1−7] Representative organic−inorganic halide perovskites show a high absorption coefficient in a UV−visible wavelength range,[8] tunable band gap,[9] large charge carrier mobility,[10,11] long charge carrier recombination lifetime,[12,13] and thus long charge carrier diffusion length,[3,14,15] unique defect tolerance property,[16] and so on. Solution processes for perovskite solar cells also offer a low-cost and high-throughput way to fabricate large area solar modules for commercialization.[17−19] However, one of the biggest obstacles faced by the commercialization of this technology is the instability of solar cell devices, which are caused by the photobleaching effect, moisture, and oxygen-induced degradation, ion migration of organic−inorganic hybrid perovskite, and so on.[20−24]

Many efforts have been dedicated to improve the stability of perovskite films or devices toward long-term operation,[20,25,26] while the perovskite degradation can actually start from precursor solution.[22,27] Unfortunately, very limited attention has been paid to the precursor solution stability upto so far. Although perovskite devices can be fabricated by a solvent-free method like vapor deposition,[28] solution processes offer unprecedented high throughput for scaling up the devices into modules for commercialization in addition to being low cost.[18,19] Perovskite solution is typically prepared by dissolving perovskite precursor ions into solvents where their chemical reactivity is often higher compared to perovskite films. Therefore, it is necessary to investigate the stability of the perovskite precursor in solution. Light is expected to play an important role that initializes and accelerates device and film degradation.[29−32] In addition, it is also reported that light induces more nucleation sites during film forming, which changes the perovskite crystallization processes and thus film morphology.[33] However, it is still not clear whether light will have any impact on perovskite precursor solution, while it is also important to the device reproducibility from different batches.

Methylammonium lead iodide ($MAPbI_3$) has been the one main material among the perovskite material family,[34−37] while its optical band gap of 1.55 eV is still too wide to match the solar spectrum for optimal device efficiency. In addition, MA ions are volatile during thermal annealing, resulting in poor device stability.[38−44] Formamidinium (FA) ions, which have a

Received: December 10, 2019
Revised: February 26, 2020
Published: March 2, 2020

larger molecular weight, are often used to replace MA^+ ions for reduced band gap and improved thermal stability.[45] Although $FAPbI_3$ easily transforms to yellow phase at room temperature,[46] incorporating some amount of Cs^+ ions and Br^- ions has been demonstrated to be an effective strategy to stabilize the black phase perovskite at room temperature.[47−51] This yields a widely used composition of $Cs_{0.05}$ $FA_{0.81}MA_{0.14}$ $PbI_{2.55}Br_{0.45}$ (CFM) for efficient and stable solar cell devices.[52−56] The corresponding devices are slightly more efficient but much more thermally stable.[20,21,26,48]

In this contribution, we studied the stability of the CFM perovskite solution under illumination and found that −CH═NH double bonds of FA^+ ions in perovskite solution gradually changed to −CH═O under light, which resulted in deteriorated device performance. Degradation mechanism is proposed to highlight the light impact on redox reactions of perovskite precursor ions. Solar cell devices were also fabricated to confirm the corresponding degradation.

DEGRADATION MECHANISM OF FA^+ IONS IN PEROVSKITE SOLUTION

Degradation of the FA-containing perovskite solution was first observed when we grew an $FAPbBr_3$ single crystal from solution processes, when we often observed black materials formed in the $FAPbBr_3$ single crystals grown for several days, as shown in Figure 1a. Studying these black materials under optical microscopy in transmission mode shows that the black substance is embedded inside the single crystals rather than on the crystal surface (see Figure 1b). To identify what the black substance is, we first dissolved the $FAPbBr_3$ single crystals back into the dimethylformamide (DMF) solvent, and the insoluble black substance was left at the bottom of the solution. We then washed the black substance with DMF several times and then conducted X-ray powder diffraction (XRD) measurements. The XRD result in Figure 1c indicates that the black substance is metallic lead (Pb). The formation of metallic Pb was reported to be bad for perovskite solar cells and other photoelectric devices.[57,58] This indicates that the perovskite precursor ions gradually decompose in solution during the crystals' growth. We noticed that Pb metal is not observed if $FAPbBr_3$ single crystals are grown by keeping them in dark conditions, indicating the function of light in the precursor degradation. In striking contrast, we did not observe Pb metal when we grew the $MAPbBr_3$ single crystals even under strong light.[10,11]

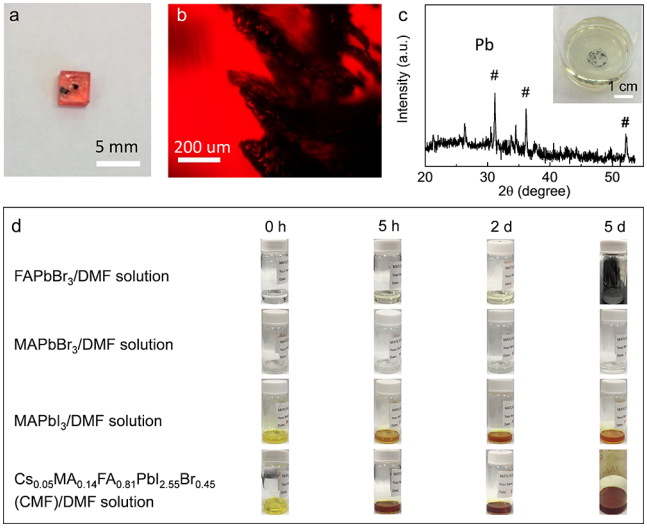

Figure 1. (a) Photo of the black substance grown in the $FAPbBr_3$ single crystal. (b) Microscopy image of the black substance in the $FAPbBr_3$ single crystal in transmission mode. (c) XRD spectrum of the black substance collected from the $FAPbBr_3$ single crystal. The inset is the photo of the black substance in the DMF solvent. The black substance is collected after the $FAPbBr_3$ single crystal is dissolved in the DMF solvent. (d) Photos of the perovskite solution soaked under AM 1.5 G light for 0 h, 5 h, 2 days, and 5 days. Perovskite solutions are $FAPbBr_3$/DMF, $MAPbBr_3$/DMF, $MAPbI_3$/DMF, and $Cs_{0.05}MA_{0.14}FA_{0.81}PbI_{2.55}Br_{0.45}$ (CFM)/DMF solutions.

To understand the perovskite solution degradation, we soaked $FAPbBr_3$ and $MAPbBr_3$ solutions under simulated sun light with an intensity of 100 mW/cm^2. The color of $FAPbBr_3$ solution gradually changes into light yellow after light soaking for 5 h, as shown in Figure 1d, and the black Pb metal showed up after 5 days, while there is no color change or Pb metal showing up from the $MAPbBr_3$ perovskite solution under the same experimental condition. This indicates that FA^+ ions participate the reduction of Pb^{2+} ions. Different from MA^+ ions, FA^+ ions have −CH═NH double bonds, which are chemically more reactive than $-CH_2-NH_2$ single bonds. Fourier-transform infrared (FTIR) spectroscopy with an attenuated total reflection (ATR) accessory was used to inspect the degradation of FA^+ ions. The FTIR spectra of the $FAPbBr_3$ powder and DMF solvent show the characteristic stretching vibration peaks of −CH═NH and −CH═O (see Figure 2a). Strong peaks located at 1716 and 1650 cm^{-1} are assigned to the stretch vibration of −CH═NH and −CH═O double bonds, respectively.[57,59] We then inspected the light-induced degradation processes of $FAPbBr_3$ in DMF by FTIR measurements. As shown in Figure 2b, changes of the two FTIR peaks, one at 3460 cm^{-1} and the other at 1720 cm^{-1}, are observed during light soaking. The broad peak at 3460 cm^{-1} is often assigned to the stretch vibration of O−H or N−H bonds.[59] It is interesting that the intensity of the 3460 cm^{-1} peak first increased during 3 h of illumination and then gradually decreased, indicating a generation and followed degradation of the organic group that is rich in O−H or N−H bonds. At the same time, we also observed a gradually reduced peak intensity at around 1720 cm^{-1}, as shown in Figure 2c, despite the fact that another strong peak of −CH═O double bonds from DMF is very close by.[60] To exclude the impact of the DMF solvent, we dissolved the $FAPbBr_3$ perovskite into the dimethyl sulfoxide (DMSO) solvent since there is no −CH═O double bonds in DMSO. In this way, we can clearly inspect the degradation of −CH═NH double bonds from the FTIR spectra. As shown in Figure 3a, the FTIR peak intensity of −CH═NH bonds from FA^+ ions decreases, and new −CH═O bonds show up at the same time, which confirms the conversion of −CH═NH to −CH═O.

The light-induced FA^+ ion degradation process is proposed to be through the redox reaction participated by organic −CH═NH bonds and inorganic $PbBr_2$. The redox reaction then takes places upon light activation, and Pb^{2+} ions are reduced to produce Pb metal in a similar way with the redox reaction between −CH═CH− double bonds and potassium permanganate(VII; Mn^{7+}).[61] Mn^{7+} can be reduced to Mn^{2+} or Mn^{4+}, depending on the reaction conditions as one typical example of metal ion reduction. Finally, −CH═NH bonds are oxidized, generating small molecular containing −CH═O bonds, such as formamide ions, ammonium formate, form-

https://dx.doi.org/10.1021/acs.chemmater.9b05101
Chem. Mater. XXXX, XXX, XXX−XXX

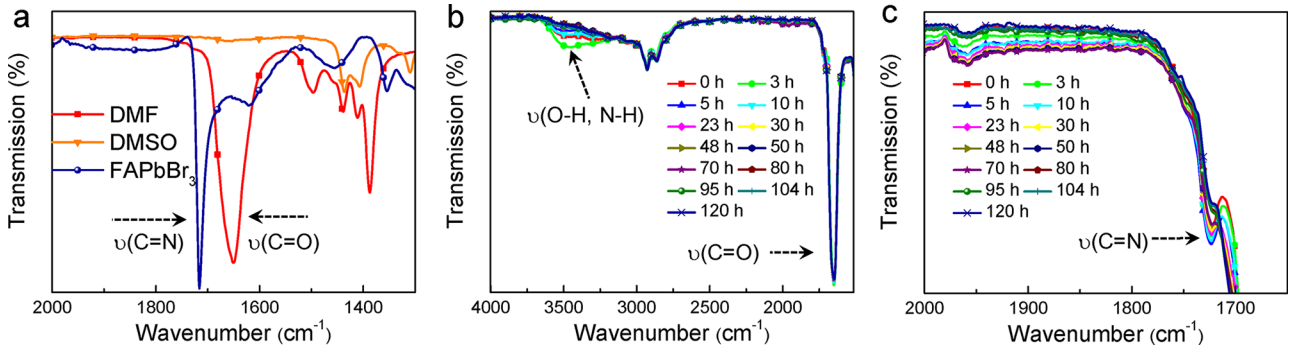

Figure 2. (a) FTIR spectra of the $FAPbBr_3$ single-crystal powder and DMF. (b) FTIR spectra of $FAPbBr_3$/DMF solution after light soaking of different periods, and the solution is prepared by dissolving FABr and $PbBr_2$ into the DMF solution. (c) Enlarged FTIR spectra of $FAPbBr_3$/DMF solution after light soaking of different periods to highlight the stretching vibration peak of −CH═NH double bonds.

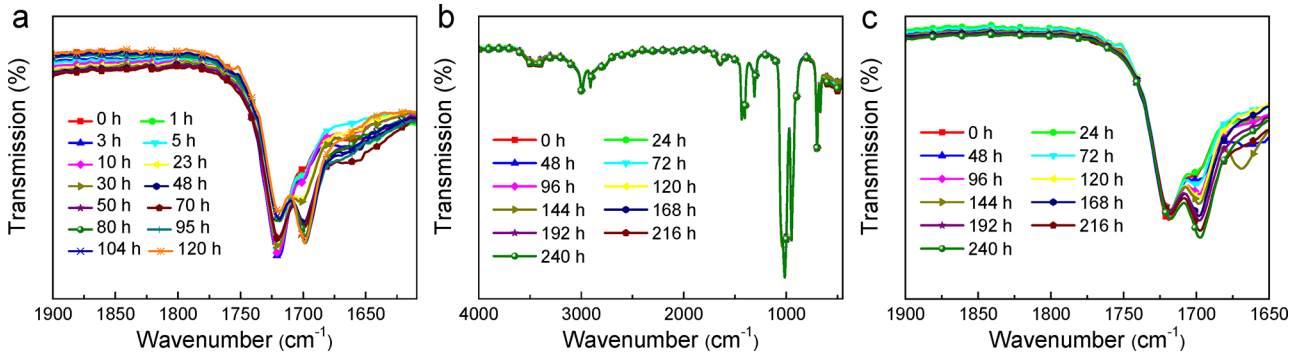

Figure 3. (a) FTIR spectra of $FAPbBr_3$/DMSO solution after light soaking of different periods. (b) FTIR spectra of $MAPbBr_3$/DMSO solution after light soaking of different periods. (c) FTIR spectra of $Cs_{0.05}MA_{0.14}FA_{0.81}PbI_{2.55}Br_{0.45}$ (CFM)/DMSO solution after light soaking of different periods.

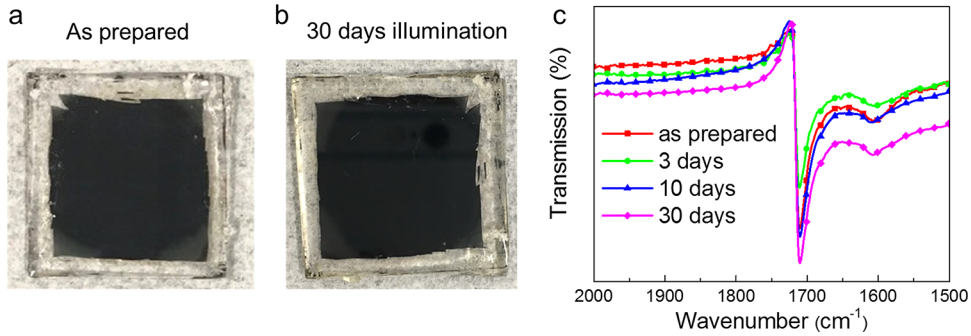

Figure 4. (a) Photo of the CFM perovskite film as prepared, which is encapsulated by a cover glass and epoxy. (b) Photos of the CFM perovskite film after 1 sun light soaking for 30 days. (c) FTIR spectra of the CFM perovskite film powder after light soaking of different periods.

aldehyde or formic acid, etc. In contrast, the FTIR spectra of $MAPbBr_3$/DMSO solution almost overlap with each other as time under 1 sun light soaking condition (see Figure 3b), and this is attributed to the absence of −CH═NH double bonds in MA^+ ions.

Considering the fact that FA^+ ions are broadly used in perovskite solar cells, it is a major concern if the perovskite solution for solar cells also degrades under light. We soaked CFM/DMFand $MAPbI_3$/DMF solutions under 1 sun light for comparison. The colors of $MAPbI_3$/DMF solution changed into dark red after 5 h (see Figure 1), and the red color should originate from the generation of iodine due to the decomposition of PbI_2 under light.[62] Meanwhile, the color of the CFM/DMF solution is darker than the $MAPbI_3$/DMF solution after light soaking, which should result from the degradation of FA^+ ions, in addition to the iodine-induced color change. We then performed the FTIR test on the CFM solution to confirm the FA^+ ion degradation under light (see Figure 3c). Since there is no Pb metal observed in the CFM perovskite solution after light soaking, we propose another degradation process. The produced iodine serves as catalysis in this reaction like many other organic reactions.[63−65] −CH═NH double bonds of FA^+ ions are directly activated in the presence of iodine catalysis and light, and then, further oxidation reaction occurs, producing −CH═O bonds.

After demonstrating the light-induced degradation of perovskite solution for solar cells, we then examined the perovskite film stability to see whether FA^+ ions in solid-state perovskite films also oxidize under light. We spin-coated CFM perovskite films on a glass in a glovebox and encapsulated them

https://dx.doi.org/10.1021/acs.chemmater.9b05101
Chem. Mater. XXXX, XXX, XXX−XXX

Table 1. Summary of the Device Performance for Perovskite Solution with Different Light Aging Time

perovskite solution	aging time[a]	J_{sc} (mA cm^{-2})	V_{oc} (V)	FF (%)	PCE (%)
$Cs_{0.05}MA_{0.14}FA_{0.81}PbI_{2.55}Br_{0.45}$	w/o	22.5	1.06	81.6	19.5
	dark 96 h	22.4	1.06	80.1	19.0
	dark 192 h	22.9	1.06	78.6	19.1
	light 96 h	21.4	1.08	61.8	14.3
	light 192 h	21.5	1.08	58.6	13.6
$MAPbI_3$	w/o	22.8	1.12	77.0	19.6
	dark 96 h	21.9	1.12	77.5	19.0
	dark 192 h	22.0	1.08	80.0	19.0
	light 96 h	21.4	1.02	71.5	15.6
	light 192 h	21.5	1.04	71.1	15.9

[a]The aging light we used is the ambient light with an intensity of 200 μW cm^{-2}.

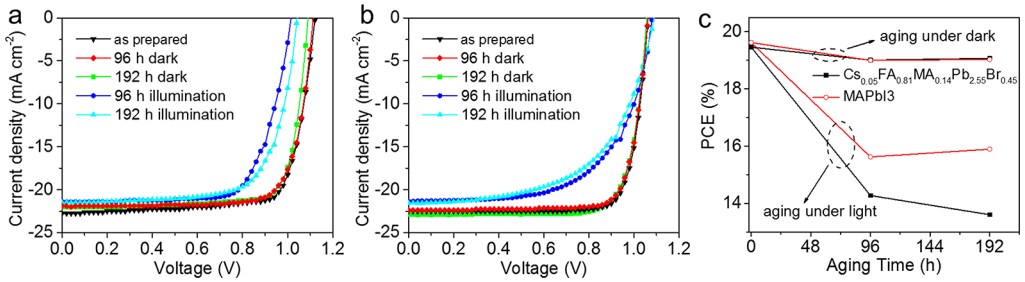

Figure 5. (a) Current density−voltage (J−V) characteristics of $MAPbI_3$ devices with different perovskite solution aging history. (b) Current density−voltage (J−V) characteristics of CFM devices with different perovskite solution aging history. (c) Evolution of PCE of $MAPbI_3$ and CFM devices regarding their perovskite solution aging history.

with a cover glass on top and epoxy for sealing. The sealed films were soaked under 1 sun light; the photos of perovskite films before and after light soaking are shown in Figure 4a,b. No obvious difference can be observed by naked eyes even after the films were soaked under 1 sun light for 30 days, and the perovskite films were then scratched for FTIR measurement. Figure 4c plots the FTIR spectra of CFM perovskite films with different light soaking periods as 3, 10, and 30 days, and we found that the stretch vibration peak of −CH═NH double bonds remains the same with that of as-prepared films. In addition, no peaks of −CH═O double bonds show up after light soaking, indicating no oxidization of FA^+ ions in solid films. This may be caused by the absence of moisture and the much lower ion migration rate in the solid film compared to that in perovskite solution and thus much lower chemical reactivity in the perovskite film. The excellent film stability also benefits from a mature encapsulation technique, although this preliminary study on film stability does not exclude the surface oxidization of a solid perovskite film.

DEVICE PERFORMANCE IMPACTED BY LIGHT AGING ON PEROVSKITE SOLUTION

To verify the impact of the FA^+ ion degradation on perovskite solar cell efficiency, we fabricated solar cell devices from CFM and $MAPbI_3$ solution with different light soaking history. $MAPbI_3$ is used for control because it does not have FA ions. The light-induced $MAPbI_3$ solution degradation should be mainly caused by the generation of iodine. Meanwhile, light-induced CFM solution degradation is a synergy effect between generated iodine and degraded −C═O molecules contained therein, indicating more film defects from the degraded CFM solution. Since solution-processed solar cell devices are often fabricated under ambient light conditions, we aged the perovskite solution under ambient light with an intensity of 200 μW cm^{-2}, rather than 1 sun light, to see its impact to the device performance. Also, we aged the CFM solution and $MAPbI_3$ solution under dark for comparison.

The planar perovskite solar cells in this study were structured as indium tin oxide (ITO)/poly[bis(4-phenyl)(2,4,6-trimethylphenyl)amine] (PTAA)/$MAPbI_3$ or CFM/fullerene (C_{60})/2,9-dimethyl-4,7-diphenyl-1,10-phenanthroline (BCP)/copper (Cu); the device performance is summarized in Table 1. This p−i−n planar heterojunction configuration gives an average PCE of 19.6% for $MAPbI_3$ and 19.5% CFM devices from fresh perovskite solutions, as shown in Figure 5a,b. Both $MAPbI_3$ and CFM solutions were stable after aging in the dark for ∼200 h, and the corresponding photovoltaic devices still show PCEs over 19%. In comparison, the device degraded dramatically when the perovskite solution was light-soaked. After light soaking of the $MAPbI_3$ perovskite solution for 96 h, the efficiency of the corresponding device drops from 19.6 to 15.6% in Figure 5c, which mainly results from the iodine interstitials or iodine vacancies. Nevertheless, the PCE device stabilizes to 15.9% after the perovskite solution was soaked under light for 192 h. In strong contrast, the PCE of the CFM device drastically drops to 14.3% after light soaking of CFM solution for 96 h and further degraded to 13.6% after 192 h. This continuous degradation resulted not only from the generation of iodine in perovskite solution but also the degradation of FA^+ ions, which leads to significant loss of FF from 81.6 to 58.6%. Meanwhile, the $MAPbI_3$ device still maintains a high FF of 71.1% after light soaking for ∼200 h.

In conclusion, we demonstrated that the light-induced FA^+ ion degradation process in perovskite precursor solution and the −CH═NH double bonds of FA^+ ions are oxidized to −CH═O double bonds as an irreversible degradation. In Br^- ion abundant conditions, Pb^{2+} is reduced to metallic Pb under 1 sun light intensity, and for the I^- ion-based perovskite

https://dx.doi.org/10.1021/acs.chemmater.9b05101
Chem. Mater. XXXX, XXX, XXX−XXX

precursor solution, I^- ions, rather than Pb^{2+} ions, participate the redox reactions with FA^+ ions. We also discovered that the perovskite film with the same composition is much more stable under light soaking, and no obvious decomposition of FA^+ ions is observed. Although light soaking of precursor solution under ambient light does not impair the device efficiency too much, this study arouses attention that the perovskite precursor solution is also of importance to device performance, which should be carefully taken care of during storage to avoid strong light illumination. In a future study, an additive with a suitable redox capacity can be developed to stabilize the FA^+ ion-based perovskite solution by doping, and the chemical reactivity of the redox additive, which acts as a sacrificial substance, should be higher than the −C═N− double bonds of FA^+ ions. This allows a wider operation window for future commercialization production.

METHODS

Device Fabrication. One-step-processed $MAPbI_3$ and $Cs_{0.05}MA_{0.14}FA_{0.81}PbI_{2.55}Br_{0.45}$ perovskites were fabricated by the anti-solvent extraction approach in the N_2 glovebox. The hole transport layer (HTL), poly[bis(4-phenyl) (2,4,6-trimethylphenyl)-amine] (PTAA), with a concentration of 2 mg/mL dissolved in toluene was spin-coated at a speed of 6000 rpm for 35 s and then annealed at 100 °C for 10 min. To improve the wetting property of the perovskite precursor on the PTAA film, the PTAA-coated ITO substrate was prewetted by spinning 50 μL of DMF at 4000 rpm for 8 s. Then, 100 μL of perovskite precursor solution was spun onto PTAA at 2000 rpm for 2 s and 4000 rpm for 20 s; the sample was quickly washed with 135 μL of toluene at 13 s of the second-step spin coating. Subsequently, the sample was annealed at 65 °C for 10 min and 100 °C for 10 min. The devices were finished by thermally evaporating C_{60} (30 nm), BCP (8 nm), and copper (80 nm) in sequential order.

Characterization. FTIR was characterized by using Spectrum Two FTIR of PerkinElmer with universal attenuated total reflectance (ATR) (Single Reflection Diamond). Simulated AM 1.5G irradiation (100 mW cm^{-2}) was produced by a Newport Sol3A solar simulator with a 450 W xenon source and 2 × 2 in. illuminated area for current−voltage measurements. The light intensity was calibrated by the reference cell and meter, which consists of a readout device and a 2 × 2 cm calibrated solar cell made of monocrystalline silicon. The photocurrent was recorded by a Keithley Model 2400 SourceMeter with a scanning rate of 0.1 V s^{-1}. The steady-state V_{oc} and J_{sc} were measured by zero bias current and zero bias voltage versus time, respectively. XRD measurements were performed with a Rigaku D/Max-B X-ray diffractometer with Bragg−Brentano parafocusing geometry, a diffracted beam monochromator, and a conventional cobalt target X-ray tube was set to 40 kV and 30 mA.

AUTHOR INFORMATION

Corresponding Author

Jinsong Huang − *Department of Applied Physical Sciences, University of North Carolina, Chapel Hill, North Carolina 27599, United States;* orcid.org/0000-0002-0509-8778; Email: jhuang@unc.edu

Authors

Haotong Wei − *Department of Applied Physical Sciences, University of North Carolina, Chapel Hill, North Carolina 27599, United States;* orcid.org/0000-0002-7273-6768

Shangshang Chen − *Department of Applied Physical Sciences, University of North Carolina, Chapel Hill, North Carolina 27599, United States*

Jingjing Zhao − *Department of Applied Physical Sciences, University of North Carolina, Chapel Hill, North Carolina 27599, United States*

Zhenhua Yu − *Department of Applied Physical Sciences, University of North Carolina, Chapel Hill, North Carolina 27599, United States*

Complete contact information is available at: https://pubs.acs.org/10.1021/acs.chemmater.9b05101

Author Contributions

†H.W. and S.C. contributed equally to this work. J.H. and H.W. conceived the idea and designed the experiments. H.W. conducted the FTIR in this work. S.C. contributed to most device fabrication. J.Z. did the XRD test. Z.Y. fabricated the perovskite film for the light soaking test. J.H. and H.W. wrote the paper. All authors reviewed this paper.

Notes

The authors declare no competing financial interest.

Reprints and permissions information is available online. Correspondence and requests for materials should be addressed to J.H. (jhuang@unc.edu).

ACKNOWLEDGMENTS

This work is financially supported by the Office of Naval Research under award N00014-17-1-2727 and the Defense Threat Reduction Agency under award no. HDTRA1-14-1-0030.

REFERENCES

(1) Kojima, A.; Teshima, K.; Shirai, Y.; Miyasaka, T. Organometal Halide Perovskites as Visible-Light Sensitizers for Photovoltaic Cells. *J. Am. Chem. Soc.* **2009**, *131*, 6050−6051.

(2) Huang, J.; Yuan, Y.; Shao, Y.; Yan, Y. Understanding the physical properties of hybrid perovskites for photovoltaic applications. *Nat. Rev. Mater.* **2017**, *2*, 17042.

(3) Stranks, S. D.; et al. Electron-Hole Diffusion Lengths Exceeding 1 Micrometer in an Organometal Trihalide Perovskite Absorber. *Science* **2013**, *342*, 341.

(4) Green, M. A.; Ho-Baillie, A.; Snaith, H. J. The emergence of perovskite solar cells. *Nat. Photonics* **2014**, *8*, 506.

(5) Kim, H.-S.; et al. Lead Iodide Perovskite Sensitized All-Solid-State Submicron Thin Film Mesoscopic Solar Cell with Efficiency Exceeding 9%. *Sci. Rep.* **2012**, *2*, 591.

(6) Chen, J.; Park, N.-G. Causes and Solutions of Recombination in Perovskite Solar Cells. *Adv. Mater.* **2018**, *31*, 1803019.

(7) Jiang, Q.; et al. Enhanced electron extraction using SnO_2 for high-efficiency planar-structure $HC(NH_2)_2PbI_3$-based perovskite solar cells. *Nat. Energy* **2017**, *2*, 16177.

(8) Lin, Q.; Armin, A.; Nagiri, R. C. R.; Burn, P. L.; Meredith, P. Electro-optics of perovskite solar cells. *Nat. Photonics* **2015**, *9*, 106.

(9) Filip, M. R.; Eperon, G. E.; Snaith, H. J.; Giustino, F. Steric engineering of metal-halide perovskites with tunable optical band gaps. *Nat. Commun.* **2014**, *5*, 5757.

(10) Xu, Q.; et al. Detection of charged particles with a methylammonium lead tribromide perovskite single crystal. *Nucl. Instrum. Methods Phys. Res., Sect. A* **2017**, *848*, 106−108.

(11) Wei, H.; et al. Sensitive X-ray detectors made of methylammonium lead tribromide perovskite single crystals. *Nat. Photonics* **2016**, *10*, 333.

(12) Zhai, Y.; et al. Giant Rashba splitting in 2D organic-inorganic halide perovskites measured by transient spectroscopies. *Sci. Adv.* **2017**, *3*, No. e1700704.

(13) Frohna, K.; et al. Inversion symmetry and bulk Rashba effect in methylammonium lead iodide perovskite single crystals. *Nat. Commun.* **2018**, *9*, 1829.

(14) Dong, Q.; et al. Electron-hole diffusion lengths > 175 μm in solution-grown $CH_3NH_3PbI_3$ single crystals. *Science* **2015**, *347*, 967.

(15) Wei, H.; Huang, J. Halide lead perovskites for ionizing radiation detection. *Nat. Commun.* **2019**, *10*, 1066.

(16) Steirer, K. X.; et al. Defect Tolerance in Methylammonium Lead Triiodide Perovskite. *ACS Energy Lett.* **2016**, *1*, 360−366.
(17) Jeon, N. J.; et al. Solvent engineering for high-performance inorganic−organic hybrid perovskite solar cells. *Nat. Mater.* **2014**, *13*, 897.
(18) Chen, H.; et al. A solvent- and vacuum-free route to large-area perovskite films for efficient solar modules. *Nature* **2017**, *550*, 92.
(19) Deng, Y.; et al. Surfactant-controlled ink drying enables high-speed deposition of perovskite films for efficient photovoltaic modules. *Nat. Energy* **2018**, *3*, 560−566.
(20) Saliba, M.; et al. Cesium-containing triple cation perovskite solar cells: improved stability, reproducibility and high efficiency. *Energy Environ. Sci.* **2016**, *9*, 1989−1997.
(21) Matsui, T.; et al. Compositional Engineering for Thermally Stable, Highly Efficient Perovskite Solar Cells Exceeding 20% Power Conversion Efficiency with 85 °C/85% 1000 h Stability. *Adv. Mater.* **2019**, *31*, 1806823.
(22) Wang, R.; et al. A Review of Perovskites Solar Cell Stability. *Adv. Funct. Mater.* **2019**, *29*, 1808843.
(23) Wang, Q.; et al. Scaling behavior of moisture-induced grain degradation in polycrystalline hybrid perovskite thin films. *Energy Environ. Sci.* **2017**, *10*, 516−522.
(24) Boyd, C. C.; Cheacharoen, R.; Leijtens, T.; McGehee, M. D. Understanding Degradation Mechanisms and Improving Stability of Perovskite Photovoltaics. *Chem. Rev.* **2019**, *119*, 3418−3451.
(25) Zhu, Z.; et al. Highly Efficient and Stable Perovskite Solar Cells Enabled by All-Crosslinked Charge-Transporting Layers. *Joule* **2018**, *2*, 168−183.
(26) Arora, N.; et al. Perovskite solar cells with CuSCN hole extraction layers yield stabilized efficiencies greater than 20%. *Science* **2017**, *358*, 768.
(27) Jung, M.; Ji, S.-G.; Kim, G.; Seok, S. I. Perovskite precursor solution chemistry: from fundamentals to photovoltaic applications. *Chem. Soc. Rev.* **2019**, *48*, 2011−2038.
(28) Liu, M.; Johnston, M. B.; Snaith, H. J. Efficient planar heterojunction perovskite solar cells by vapour deposition. *Nature* **2013**, *501*, 395.
(29) Wang, Z.; et al. Efficient ambient-air-stable solar cells with 2D−3D heterostructured butylammonium-caesium-formamidinium lead halide perovskites. *Nat. Energy* **2017**, *2*, 17135.
(30) Tsai, H.; et al. Light-induced lattice expansion leads to high-efficiency perovskite solar cells. *Science* **2018**, *360*, 67.
(31) Li, Y.; et al. Light-Induced Degradation of $CH_3NH_3PbI_3$ Hybrid Perovskite Thin Film. *J. Phys. Chem. C* **2017**, *121*, 3904−3910.
(32) Wei, D.; et al. Photo-induced degradation of lead halide perovskite solar cells caused by the hole transport layer/metal electrode interface. *J. Mater. Chem. A* **2016**, *4*, 1991−1998.
(33) Ummadisingu, A.; et al. The effect of illumination on the formation of metal halide perovskite films. *Nature* **2017**, *545*, 208.
(34) Quarti, C.; et al. Structural and optical properties of methylammonium lead iodide across the tetragonal to cubic phase transition: implications for perovskite solar cells. *Energy Environ. Sci.* **2016**, *9*, 155−163.
(35) Haruyama, J.; Sodeyama, K.; Han, L.; Tateyama, Y. Surface Properties of $CH_3NH_3PbI_3$ for Perovskite Solar Cells. *Acc. Chem. Res.* **2016**, *49*, 554−561.
(36) Chiang, C.-H.; Nazeeruddin, M. K.; Grätzel, M.; Wu, C.-G. The synergistic effect of H_2O and DMF towards stable and 20% efficiency inverted perovskite solar cells. *Energy Environ. Sci.* **2017**, *10*, 808−817.
(37) Holzhey, P.; et al. A chain is as strong as its weakest link − Stability study of $MAPbI_3$ under light and temperature. *Mater. Today* **2019**, *29*, 10−19.
(38) Zhou, Z.; et al. Methylamine-Gas-Induced Defect-Healing Behavior of $CH_3NH_3PbI_3$Thin Films for Perovskite Solar Cells. *Angew. Chem., Int. Ed.* **2015**, *54*, 9705−9709.
(39) Nagabhushana, G. P.; Shivaramaiah, R.; Navrotsky, A. Direct calorimetric verification of thermodynamic instability of lead halide hybrid perovskites. *Proc. Natl. Acad. Sci. U. S. A.* **2016**, *113*, 7717.
(40) Qiu, T.; Hu, Y.; Bai, F.; Miao, X.; Zhang, S. Improved performance and stability of perovskite solar cells by incorporating gamma-aminobutyric acid in $CH_3NH_3PbI_3$. *J. Mater. Chem. A* **2018**, *6*, 12370−12379.
(41) Turren-Cruz, S.-H.; Hagfeldt, A.; Saliba, M. Methylammonium-free, high-performance, and stable perovskite solar cells on a planar architecture. *Science* **2018**, *362*, 449.
(42) Wang, F.; et al. Organic Cation-Dependent Degradation Mechanism of Organotin Halide Perovskites. *Adv. Funct. Mater.* **2016**, *26*, 3417−3423.
(43) Futscher, M. H.; et al. Quantification of ion migration in $CH_3NH_3PbI_3$ perovskite solar cells by transient capacitance measurements. *Mater. Horiz.* **2019**, *6*, 1497−1503.
(44) Charles, B.; Dillon, J.; Weber, O. J.; Islam, M. S.; Weller, M. T. Understanding the stability of mixed A-cation lead iodide perovskites. *J. Mater. Chem. A* **2017**, *5*, 22495−22499.
(45) Eperon, G. E.; et al. Formamidinium lead trihalide: a broadly tunable perovskite for efficient planar heterojunction solar cells. *Energy Environ. Sci.* **2014**, *7*, 982−988.
(46) Han, Q.; et al. Single Crystal Formamidinium Lead Iodide ($FAPbI_3$): Insight into the Structural, Optical, and Electrical Properties. *Adv. Mater.* **2016**, *28*, 2253−2258.
(47) Liu, T.; et al. High-Performance Formamidinium-Based Perovskite Solar Cells via Microstructure-Mediated δ-to-α Phase Transformation. *Chem. Mater.* **2017**, *29*, 3246−3250.
(48) Pellet, N.; et al. Mixed-Organic-Cation Perovskite Photovoltaics for Enhanced Solar-Light Harvesting. *Angew. Chem., Int, Ed.* **2014**, *53*, 3151−3157.
(49) Yi, C.; et al. Entropic stabilization of mixed A-cation ABX_3 metal halide perovskites for high performance perovskite solar cells. *Energy Environ. Sci.* **2016**, *9*, 656−662.
(50) Ni, X.; et al. Effect of Br content on phase stability and performance of $H_2N{=}CHNH_2Pb(I_{1-x}Br_x)_3$ perovskite thin films. *Nanotechnology* **2019**, *30*, 165402.
(51) Chen, L.; et al. Toward Long-Term Stability: Single-Crystal Alloys of Cesium-Containing Mixed Cation and Mixed Halide Perovskite. *J. Am. Chem. Soc.* **2019**, *141*, 1665−1671.
(52) Rong, Y.; et al. Challenges for commercializing perovskite solar cells. *Science* **2018**, *361*, eaat8235.
(53) Kim, H.-S.; Hagfeldt, A.; Park, N.-G. Morphological and compositional progress in halide perovskite solar cells. *Chem. Commun.* **2019**, *55*, 1192−1200.
(54) Sun, Y.; Peng, J.; Chen, Y.; Yao, Y.; Liang, Z. Triple-cation mixed-halide perovskites: towards efficient, annealing-free and air-stable solar cells enabled by $Pb(SCN)_2$ additive. *Sci. Rep.* **2017**, *7*, 46193.
(55) Ono, L. K.; Juarez-Perez, E. J.; Qi, Y. Progress on Perovskite Materials and Solar Cells with Mixed Cations and Halide Anions. *ACS Appl. Mater. Interfaces* **2017**, *9*, 30197−30246.
(56) Wang, Z.; et al. High irradiance performance of metal halide perovskites for concentrator photovoltaics. *Nat. Energy* **2018**, *3*, 855−861.
(57) Wang, L.; et al. A Eu^{3+}-Eu^{2+} ion redox shuttle imparts operational durability to Pb-I perovskite solar cells. *Science* **2019**, *363*, 265.
(58) Tan, Z.-K.; et al. Bright light-emitting diodes based on organometal halide perovskite. *Nat. Nanotechnol.* **2014**, *9*, 687.
(59) Zhou, Z.; Pang, S.; Ji, F.; Zhang, B.; Cui, G. The fabrication of formamidinium lead iodide perovskite thin films via organic cation exchange. *Chem. Commun.* **2016**, *52*, 3828−3831.
(60) Cao, X. B.; et al. High quality perovskite films fabricated from Lewis acid−base adduct through molecular exchange. *RSC Adv.* **2016**, *6*, 70925−70931.
(61) Dash, S.; Patel, S.; Mishra, B. K. Oxidation by permanganate: synthetic and mechanistic aspects. *Tetrahedron* **2009**, *65*, 707−739.
(62) Aristidou, N.; et al. The Role of Oxygen in the Degradation of Methylammonium Lead Trihalide Perovskite Photoactive Layers. *Angew. Chem., Int. Ed.* **2015**, *54*, 8208−8212.

https://dx.doi.org/10.1021/acs.chemmater.9b05101
Chem. Mater. XXXX, XXX, XXX−XXX

(63) Itoh, A.; Kodama, T.; Masaki, Y.; Inagaki, S. Oxidative Cleavage of the Double Bonds of Styrenes with a Combination of Mesoporous Silica FSM-16 and I_2 under Photoirradiation. *Synlett* **2002**, *2002*, 0522−0524.
(64) Gogoi, P.; Sarmah, G. K.; Konwar, D. DMSO/N_2H_4·H_2O/I_2/H_2O/CH_3CN: A New System for Selective Oxidation of Alcohols in Hydrated Media. *J. Org. Chem.* **2004**, *69*, 5153−5154.
(65) Gangloff, A. R.; Judge, T. M.; Helquist, P. Light-induced, iodine-catalyzed aerobic oxidation of unsaturated tertiary amines. *J. Org. Chem.* **1990**, *55*, 3679−3682.

https://dx.doi.org/10.1021/acs.chemmater.9b05101
Chem. Mater. XXXX, XXX, XXX−XXX